REPORT DOCUMENTATION PAGE

Form Approved
OMB No. 0704-0188

1. REPORT DATE (DD-MM-YYYY)	2. REPORT TYPE	3. DATES COVERED (From - To)
	Technical Papers	

4. TITLE AND SUBTITLE

Please see attached

5a. CONTRACT NUMBER

5b. GRANT NUMBER

5c. PROGRAM ELEMENT NUMBER

6. AUTHOR(S)

5d. PROJECT NUMBER
2308

5e. TASK NUMBER
M19B

5f. WORK UNIT NUMBER
346058

7. PERFORMING ORGANIZATION NAME(S) AND ADDRESS(ES)

Air Force Research Laboratory (AFMC)
AFRL/PRS
5 Pollux Drive
Edwards AFB CA 93524-7048

8. PERFORMING ORGANIZATION REPORT

9. SPONSORING / MONITORING AGENCY NAME(S) AND ADDRESS(ES)

Air Force Research Laboratory (AFMC)
AFRL/PRS
5 Pollux Drive
Edwards AFB CA 93524-7048

10. SPONSOR/MONITOR'S ACRONYM(S)

11. SPONSOR/MONITOR'S NUMBER(S)
Please see attached

12. DISTRIBUTION / AVAILABILITY STATEMENT

Approved for public release; distribution unlimited.

13. SUPPLEMENTARY NOTES

14. ABSTRACT

15. SUBJECT TERMS

16. SECURITY CLASSIFICATION OF:			17. LIMITATION OF ABSTRACT	18. NUMBER OF PAGES	19a. NAME OF RESPONSIBLE PERSON
a. REPORT	b. ABSTRACT	c. THIS PAGE			Leilani Richardson
Unclassified	Unclassified	Unclassified	A		19b. TELEPHONE NUMBER (include area code) (661) 275-5015

DTIC 20030219

MEMORANDUM FOR PRS (In-House Publication)

FROM: PROI (STINFO) 11 Jan 2001

SUBJECT: Authorization for Release of Technical Information, Control Number: **AFRL-PR-ED-TP-2001-005** Ketsdever, A.; Green, A.; and Muntz, E.P., "Momentum Flux Measurements From Under Expanded Orifices"

Presentation for AIAA Aerospace Sciences Meeting **(Statement A)**
(Reno, NV, 8-11 Jan 01) (Deadline: Past)

AIAA-2001-0502

Momentum Flux Measurements from Under Expanded Orifices: Applications for Micropropulsion Systems

Andrew D. Ketsdever†
Air Force Research Laboratory
Propulsion Directorate
Edwards AFB, CA

Amanda A. Green* and E.P. Muntz‡
University of Southern California
Department of Aerospace Engineering
Los Angeles, CA

Please stay consistent throughout paper - we suggest making this one word.

ABSTRACT

The popularity of micropropulsion system development has led to renewed interest in the determination of propulsive properties of orifice flows since micronozzle expansions may suffer high viscous losses at low pressure operation. The mass flow and relative thrust through an underexpanded orifice is measured as a function of orifice stagnation pressure from 0.1 to 3.5 Torr. Nitrogen, argon, and helium propellant gases are passed through a 1.0 mm diameter orifice with a wall thickness of 0.015 mm . Near-free molecule, transitional and continuum flow regimes are studied. The relative thrust is determined by measuring the displacement of a novel thrust stand designed primarily for low operating pressure propulsion systems. It is shown that the thrust stand deflection is a function of the facility background pressure, and corrections are made to determine the deflection for a zero background pressure for a nitrogen propellant.

Nomenclature

a – speed of sound (m/sec)
A – area (m^2)
c(γ) – constant dependent on ratio of specific heats
c' – mean molecular thermal speed (m/sec)
C_D – discharge coefficient
d – diameter (m)
g – gravitational constant (= 9.8 m/sec^2)
Isp – specific impulse (sec)
k – Boltzmann's constant (= 1.38 x 10^{-23} J/K)
Kn – Knudsen Number
m – mass (kg)
$\dot{M}$ - mass flow (kg/sec)
n – number density (m^{-3})
p – pressure (Pa)
Re – Reynolds Number
r_p – radius of penetration (m)
t – thickness (m)
T – temperature (K)

α - orifice transmission probability
γ - ratio of specific heats
λ - mean free path (m)
μ - viscosity (Ns/m^2)
ρ - mass density (kg/m^3)
Δ - thrust stand deflection (arb. units)

subscripts

b – facility background
fm – free molecule
L – limit (theoretical maximum)
meas – experimentally measured
o – stagnation region
p - plenum
t – orifice or nozzle throat property
theor - theoretical

superscripts

* - orifice plane (sonic) region

1. Introduction

In recent years, micropropulsion systems have been developed to address the need for highly mobile micro- and nanospacecraft. A wide array of concepts will require the expansion of propellant gases through microscale geometries (e.g. micronozzles). Because of the volume and power restrictions associated with storing or producing high pressures on micospacecraft, many micropropulsion systems will operate at relatively low pressures in the transitional flow regime.[1] The Reynolds number gives a measure of the flow efficiency in terms of viscous losses. The Reynolds number at a nozzle throat or an orifice is given by

$$\mathrm{Re}^* = \frac{\rho^* a^* d_t}{\mu^*} \qquad (1)$$

A Lower Reynolds number implies higher viscous flow losses. Microspacecraft propulsion systems may inherently operate in low Reynolds number regions due to relatively low operating pressures and small characteristic dimensions.

Figure 1 shows the specific impulse as a function of distance through a conical micronozzle geometry with a throat diameter of $d_t = 27.7\ \mu m$. Navier-Stokes and Direct Simulation Monte Carlo numerical simulations have been performed at two different stagnation pressures $p_o = 10^6$ Pa and 10^5 Pa. For cold gas operation (T_o = 300 K), the corresponding Reynolds numbers are 1300 and 130 respectively. As Fig. 1 shows, the specific impulse at the nozzle exit is approximately 14% higher than at the nozzle throat for $\mathrm{Re}^* = 1300$. However, the specific impulse at the exit is only about 5% higher than at the nozzle throat for $\mathrm{Re}^* = 130$. The reduction of efficiency in the micronozzle geometry as the Reynolds number decreases is due to viscous losses near the nozzle walls.

There is currently a large effort being devoted to the fabrication of micronozzles with throat diameters on the order of one to tens of micrometers (microns).[3-5] As Fig. 1 indicates, nozzle expansions may not be justified when weighing the increase in performance versus fabrication complexity. At low Reynolds numbers, the micronozzle geometry may in fact degrade performance, and expansion of propellant from a simple thin walled orifice may be a good compromise between efficiency and system complexity. Some microelectromechanical systems (MEMS)-fabricated nozzle geometries involve planar or rectangular throats (i.e. not conical).[3] Numerical studies have shown that flows generated near the side walls can result in even higher inefficiencies.[6]

The flow complexities from sonic orifices have been studied for several years.[7-11] However, the determination of the thrust generated from gas expanding through an orifice is an area that has received little attention. The advent of micropropulsion systems has renewed interest in the determination of propulsive properties of orifice flows since micronozzle expansions appear to have major viscous losses.

This manuscript explores the thrust generated by an orifice expansion at relatively low Reynolds number. Besides being a propulsion system in its own right, these orifices are also being investigated as a reliable means of calibrating micro-Newton thrust stands.[12]

2. Theory

To assess the performance of the orifice expansion in terms of propulsive parameters, properties at the entrance plane of the orifice are calculated from known stagnation values. The ratios of pressure, density, temperature and velocity for inviscid flow are

$$\frac{p^*}{p_o} = \left[\frac{2}{\gamma+1}\right]^{\gamma/\gamma-1} \qquad (2)$$

$$\frac{\rho^*}{\rho_o} = \left[\frac{2}{\gamma+1}\right]^{1/\gamma-1} \qquad (3)$$

$$\rho_o = \frac{p_o m}{k T_o} \qquad (4)$$

$$\left(\frac{a^*}{a_o}\right)^2 = \frac{T^*}{T_o} = \frac{2}{\gamma+1} \qquad (5)$$

The theoretical, inviscid flow value for the orifice mass flow is

$$\dot{M} = \rho^* a^* A_t \qquad (6)$$

Viscous effects can be measured in terms of a discharge coefficient defined by

$$C_D = \frac{\dot{M}_{meas}}{\dot{M}_{theor}} \qquad (7)$$

where $\dot{M}_{theor}$ is calculated from Eq. (6). The theoretical thrust produced by the orifice is then given by

$$\Im = \dot{M}u^* + p^* A_t \qquad (8)$$

$$\Im = \left(\frac{\rho^*}{\rho_o} + \frac{p^*}{p_o} \right) A_t = c(\gamma) p_o A_t \qquad (9)$$

The constant c(γ) is equal to 1.16 and 1.14 for γ = 1.4 and 1.67 respectively. Therefore, it is expected that the thrust produced by the orifice gas flow is relatively independent of the propellant.

A measure of the propulsive efficiency is given by the specific impulse as

$$Isp^* = \frac{\Im}{\dot{M}g} = \frac{\sqrt{\frac{2(\gamma+1)}{\gamma} \frac{k}{m} T_o}}{g} \qquad (10)$$

For free molecule flow, the Knudsen number defined by

$$Kn_t = \frac{\lambda_o}{d_t} \qquad (11)$$

is relatively high (Kn ≥ 10). This is accomplished at very low stagnation pressure operation where the molecule mean free path is larger than the orifice diameter. The free molecule mass flow, thrust and specific impulse are given by

$$\dot{M}_{fm} = \alpha n \frac{n_o \bar{c}}{4} A_t = \alpha m n_o \frac{\sqrt{\frac{8kT_o}{\pi m}}}{4} A_t \qquad (12)$$

$$\Im_{fm} = \alpha \frac{p_o}{2} A_t \qquad (13)$$

$$Isp_{fm} = \sqrt{\frac{\pi}{2} \frac{k}{m} T_o} \qquad (14)$$

3. Experiment

The orifice used in this study has a diameter of d_t = 1.0 mm and a thickness of t_t = 0.015 mm giving a t/d = 0.015. For t/d = 0.015, the transmission probability (α in Eqs. (12) and (13)) is very close to unity.[13] The orifice is machined by conventional means in a Tantalum shim which is attached to an aluminum plenum as shown in Fig. 2. The aluminum plenums are attached to a torsional thrust stand shown in Fig 3. The thrust measurements involve sensing the angular displacement resulting from a torque (thrust force) applied to a damped rotary system. The present method for detecting angular deflection is to measure the linear displacement of a known radial distance using a linear voltage differential transducer (LVDT) by Macro Sensors. The total linear movement of the arm is approximately 0.5 mm for a 2mN thrust level which corresponds to less than 0.1° angular deflection. The detailed operational characteristics of this thrust stand is the topic of earlier work.[7]

The thrust stand is placed inside the CHAFF-II facility, a steel vacuum chamber pumped by a Roots blower system with a pumping speed of 2000 L/sec for nitrogen. Ultimate pressures achievable in CHAFF-II are approximately 1.0 x 10^{-4} Torr.

The propellant is introduced into the orifice plenum through an adjustable needle valve located downstream of an MKS® mass flow meter. In the experimental configuration, the mass flow meter operated in the continuum regime through the pressure range studied. Nitrogen, argon and helium are used as propellant gases in this study.

4. Results

Figure 4 shows the discharge coefficient as a function of the Reynolds number for nitrogen. At lower Reynolds number, the measured values should asymptotically approach the theoretical free molecule limit of 0.583. For the range of Reynolds number shown in Fig. 4, the orifice stagnation pressure ranges from 0.1 to 3.5 Torr. As expected, the discharge coefficient

asymptotes towards unity for higher Reynolds number.

The measured linear deflection from the thrust stand mounted LVDT is shown as a function of orifice stagnation pressure for nitrogen propellant in Fig. 5. Using Eq. (8) with the measured mass flow and stagnation pressure, the theoretical range of thrust shown in Fig. 5 is from approximately 7.9 μN (p_o = 0.1 Torr) to 430 μN (p_o = 3.5 Torr). Similar plots are shown for argon and helium in Figs. 6 and 7, respectively. Figure 8 shows the nitrogen deflection as a function of mass flow.

As seen in Fig. 9a, the data for nitrogen and argon can be fit by the same straight line as expected from Eq. (9). However, this level of agreement is only true for propellants which have a similar Reynolds number for a given stagnation pressure (i.e. similar viscous effects as a function of p_o). Because the orifice Reynolds number (Eq. (1)) is a factor of three lower for helium than nitrogen at a given stagnation pressure, it is expected that the thrust (deflection) would be somewhat lower for helium due to viscous effects as shown in Fig. 9b.

The data for helium and nitrogen are shown in Fig. 10. The discrepancy in the data is indicative of the fact that the helium flow is more rarefied (higher Knudsen number) for a given stagnation pressure. For example, for nitrogen flow at p_o = 0.1 Torr, the Knudsen number is approximately 0.5. For helium, the Knudsen number is approximately 1.4 for the same stagnation pressure. This indicates that viscous effects are more important for helium flow than nitrogen at a given stagnation pressure.

It is known that the deflection for a given orifice stagnation pressure is dependent on the background pressure of the facility. Figure 11 shows the measured deflection for given orifice stagnation pressures as a function of the chamber background pressure. The absolute deflection for a given stagnation pressure decreases as the background pressure increases. The slope and intercept of the data is used to correct the data in Fig. 5 to a zero background pressure in the following section.

5. Discussion

Indications of Rarefied Flow

Figure 12 shows the effects of rarefied flow on the measured thrust (deflection) from the orifice. For helium, the flow Knudsen number at p_o = 0.1 Torr is approximately 1.4. The helium deflection data in Fig. 12 shows the theoretical lines for free molecule and inviscid continuum thrust. The data is bounded by the free molecule and continuum solutions. At the lower operating pressure, the data closely follows the free molecular slope and tends toward the inviscid continuum solution at higher pressures. The data does not quite asymptote to the inviscid solution at the maximum Reynolds number (p_o = 3.5 Torr) of about 27.

Figure 13 shows a similar result for nitrogen propellant flows. At the higher operating pressures, the nitrogen flows closely follow the inviscid continuum solution. This is consistent with the discharge coefficient results shown in Fig. 4 which indicates a discharge coefficient near unity for $Re^* > 40$.

Facility Background Pressure Corrections

Because the facility background pressure is made up of two components (laboratory air and propellant), corrections to the thrust stand deflections can only be approximated for the nitrogen propellant cases where the propellant and the laboratory backgrounds are similar.

The mechanism for lower thrust deflection as a function of increased background pressure is shown schematically in Fig. 14. For no orifice flow, the background pressure exerts an equal force on the front and back sides of the orifice plenum (equilibrium). As flow is introduced through the orifice, the resulting jets acts like an ejector pump similar to that of the oil vapor in a vacuum diffusion pump.[13,14] Collisional "removal" of the background gas by the orifice plume results in a lower background pressure on the jet side of the plenum than on the back side. This pressure difference exerts a force on the orifice in a direction opposite of the thrust vector produced by the jet. Since the gas density in the plume is relatively high compared to the background gas density in the vicinity of the orifice, the source flow can effectively prevent background molecules from penetrating the orifice plume and striking the front surface of the orifice plenum for reasonable background pressures ($p_b < 1 \times 10^{-3}$ Torr).[15] This suggests

that the deflection as a function of the background pressure should be linear as a first order approximation as Fig. 11 indicates, or

$$\frac{d\Delta}{dp_b} = \text{constant}$$

$$\left(\Delta_{p_b=0}\right) - \left(\Delta_{p_b}\right) = p_b A_{eff} \qquad (15)$$

The effective area, A_{eff}, is a measure of the area being utilized to cause the deflection opposite to the thrust vector. Assuming that the background pressure in front of the orifice plenum is zero, the force exerted on the back side of the orifice plenum (A_p = 22.75 cm^2) is approximately 100 μN for p_b = 3.3 x 10^{-4} Torr. Therefore, the background pressure "negative thrust" effect can be a significant fraction of total measured thrust produced by the orifice.

Figure 15 shows the nitrogen thrust stand deflection for a corrected zero background pressure. This data is derived from the slopes of the deflection versus background pressure curves in Fig. 11 and the data obtained in Fig. 5.

6. Conclusions

7. Acknowledgements

The authors wish to thank Mr. Brian Bjelde for his assistance with the thrust stand and data reduction.

8. References

1. Ketsdever, A., "System Considerations and Design Options for Microspacecraft Propulsion Systems," in Micropropulsion for Small Spacecraft, AIAA Progress Series in Astronautics and Aeronautics, eds. Micci and Ketsdever, Vol. 187, 2000, pp. 139-166.

2. Ivanov, M., Markelov, G., Ketsdever, A., Wadsworth, D., "Numerical Study of Cold Gas Micronozzle Flows," AIAA paper 99-0166, January, 1999.

3. Bayt, R., Breuer, K., "Fabrication and Testing of Micron-Sized Cold-Gas Thrusters," in Micropropulsion for Small Spacecraft, AIAA Progress Series in Astronautics and Aeronautics, eds. Micci and Ketsdever, Vol. 187, 2000, pp. 381-398.

4. Janson, S., Helvajian, H., "Batch-Fabricated Microthrusters: Initial Results," AIAA paper 96-2988, July 1996.

5. Kohler, J., Jonsson, M., Simu, U., Stenmark, L., "Mass Flows of Fluidic Components for Cold Gas Thruster Systems," Micro/Nanotechnology for Space Applications, Pasadena, CA, April 1999.

6. Alexeenko, A., Gimelshein, S., Levin, D., Collins, R., "Numerical Modeling of Axisymmetric and Three-Dimensional Flows in MEMS Nozzles," AIAA paper 00-3668, July 2000.

7. Ashkenas, H., Sherman, F., "The Structure and Utilization of Supersonic Free Jets in Low Density Wind Tunnels," in Rarefied Gas Dynamics, Proceedings of the 4th International Symposium, ed. de Leeuw, Vol. 2, 1966, pp. 84-105.

8. Sreekanth, A., Prasad, A., Prasad, D., "Numerical and Experimental Investigations of Rarefied Gas Flows Through Nozzles and Composite Systems," in Rarefied Gas Dynamics, Proceedings of the 17th International Symposium, ed. Beylich, 1991, pp. 987-994.

9. Rebrov, A., "Free Jets in Vacuum Technologies," J. Vac. Sci. and Technol. A, to be published.

10. Meyer, J., "Measurements of Particle Densities and Flow Directions in Freejets and in Background Gas," in Rarefied Gas Dynamics: Experimental Techniques and Physical Systems, AIAA Progress Series in Astronautics and Aeronautics, eds. Shizgal and Weaver, Vol. 158, 1994, pp. 333-341.

11. Livesey, R., "Flow of Gases Through Tubes and Orifices," in Foundations of Vacuum Science and Technology, ed. Lafferty, 1998, pp. 81-140.

12. Tew, J., VanDenDriessche, J., Lutfy, F., Muntz, E.P., Wong, J., Ketsdever, A., "A Thrust Stand Designed for Performance Measurements of the Free Molecule Micro-Resistojet," AIAA paper 2000-3673, July 2000.

13. Dayton, B., "Diffusion and Diffusion-Ejector Pumps," in Foundations of Vacuum Science and Technology, ed. Lafferty, 1998, pp. 175-232.

14. Rebrov, A., "Studies on Physical Gas Dynamics of Jets as Applied to Vacuum Pumps," in Rarefied Gas Dynamics, Proceedings of the 15th International Symposium, ed. Teubner, 1986, pp. 455-473.

15. Muntz, E.P., Hamel, B.B., Maguire, B.L., "Some Characteristics of Exhaust Plume Rarefaction," AIAA J., Vol. 8, No. 9, 1970, pp. 1651-1658.

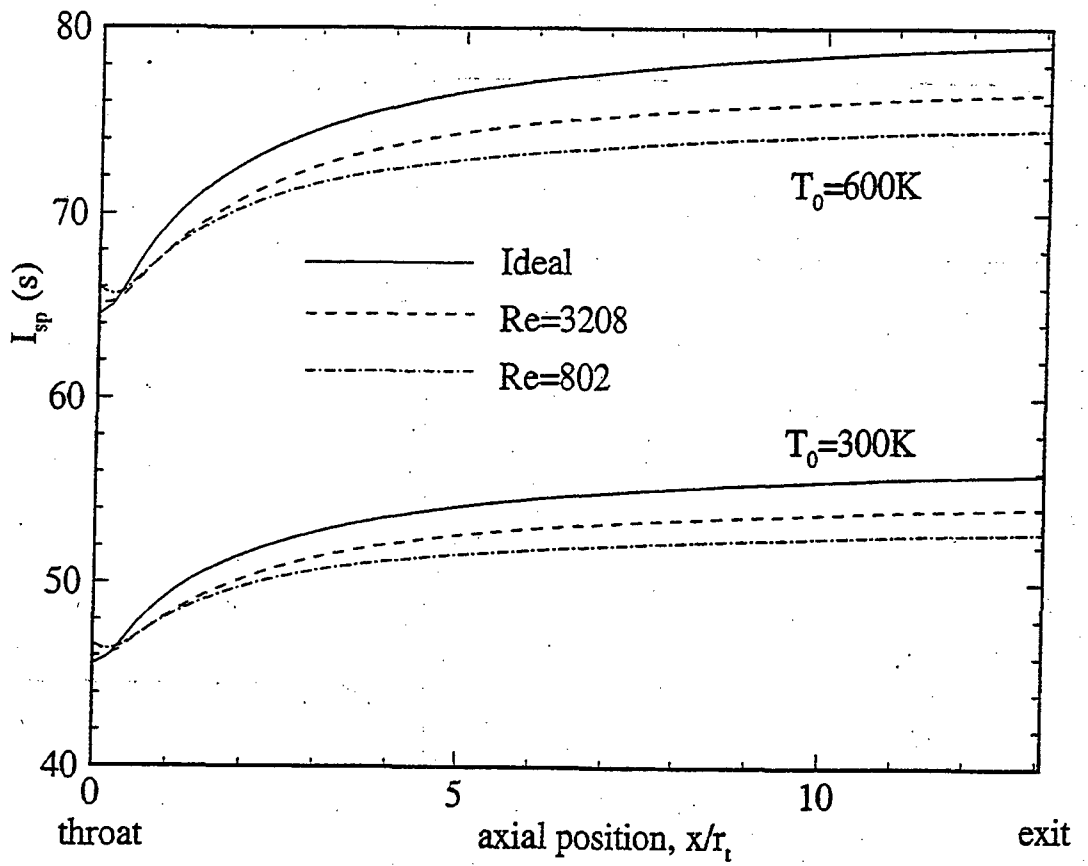

~~Fig. 2~~

Suggest using titles / captions to identify each figure

Fig. 1

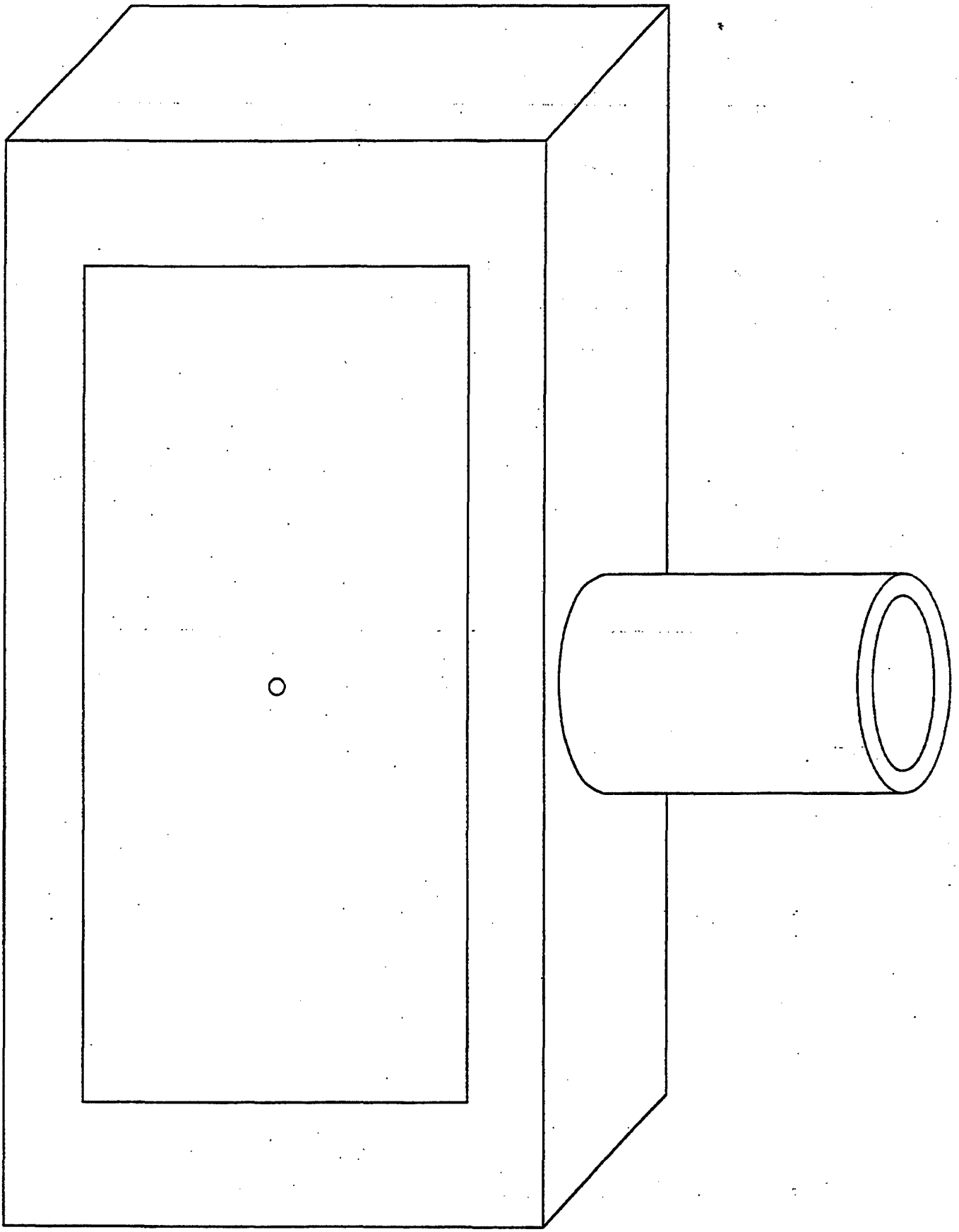

Fig. 2

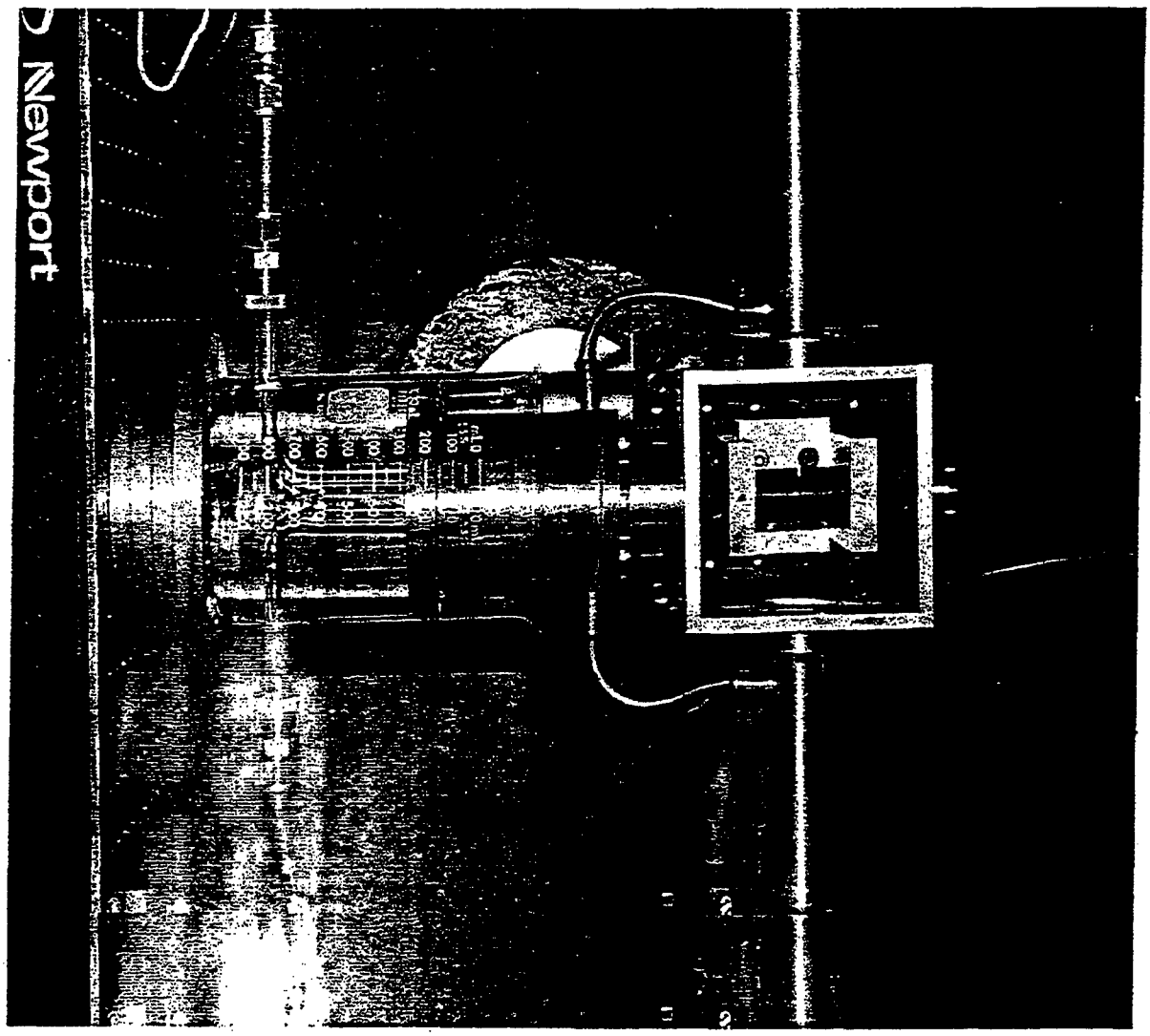

Fig. 3

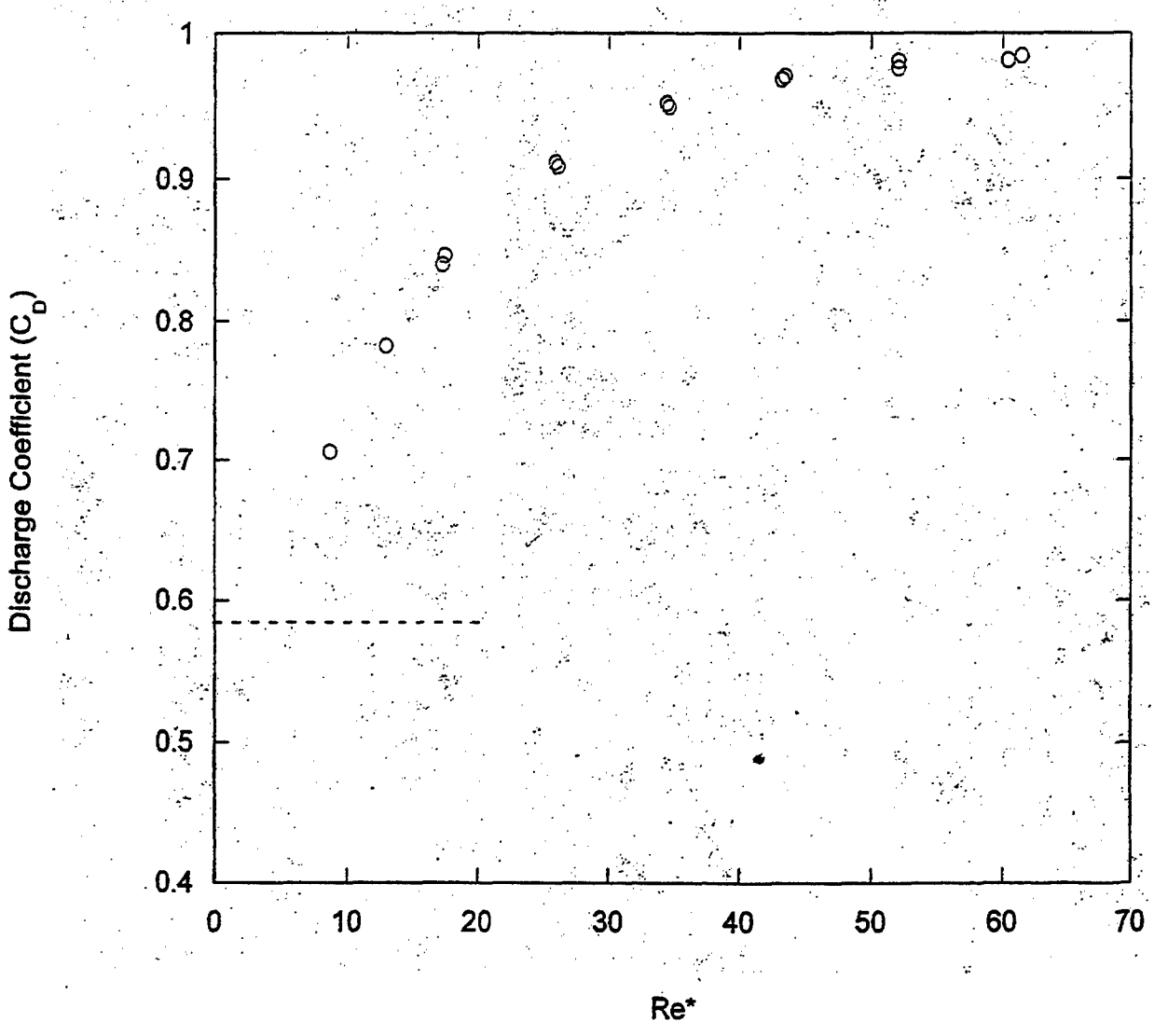
Discharge Coefficient (C_D)
1
0.9
0.8
0.7
0.6
0.5
0.4
0
10
20
30
40
50
60
70
Re*

Fig. 4

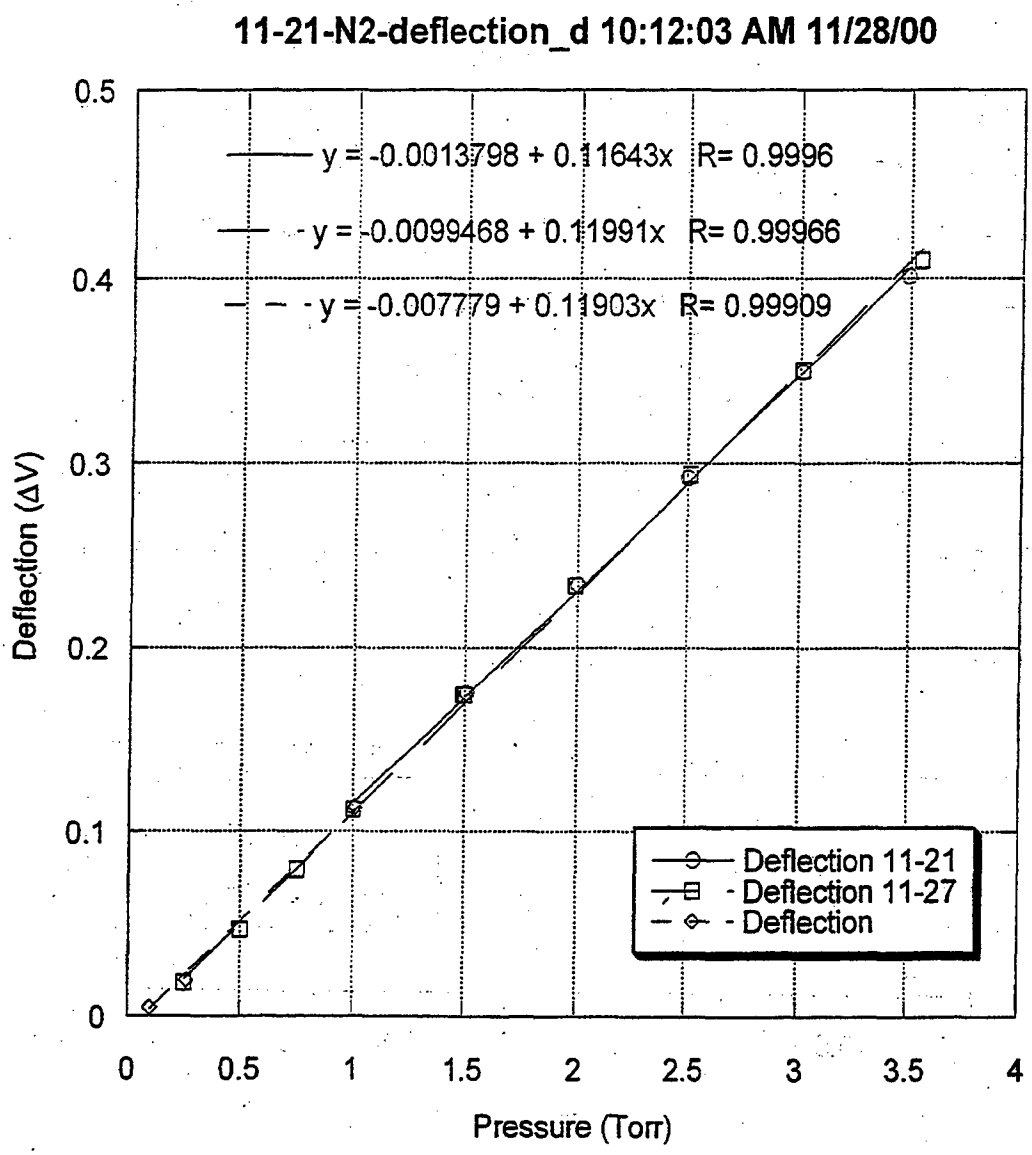
11-21-N2-deflection_d 10:12:03 AM 11/28/00
y = -0.0013798 + 0.11643x R= 0.9996
y = -0.0099468 + 0.11991x R= 0.99966
y = -0.007779 + 0.11903x R= 0.99909
Deflection (ΔV)
Pressure (Torr)
0
0.1
0.2
0.3
0.4
0.5
0.5
1
1.5
2
2.5
3
3.5
4
Deflection 11-21
Deflection 11-27
Deflection

Fig. 5

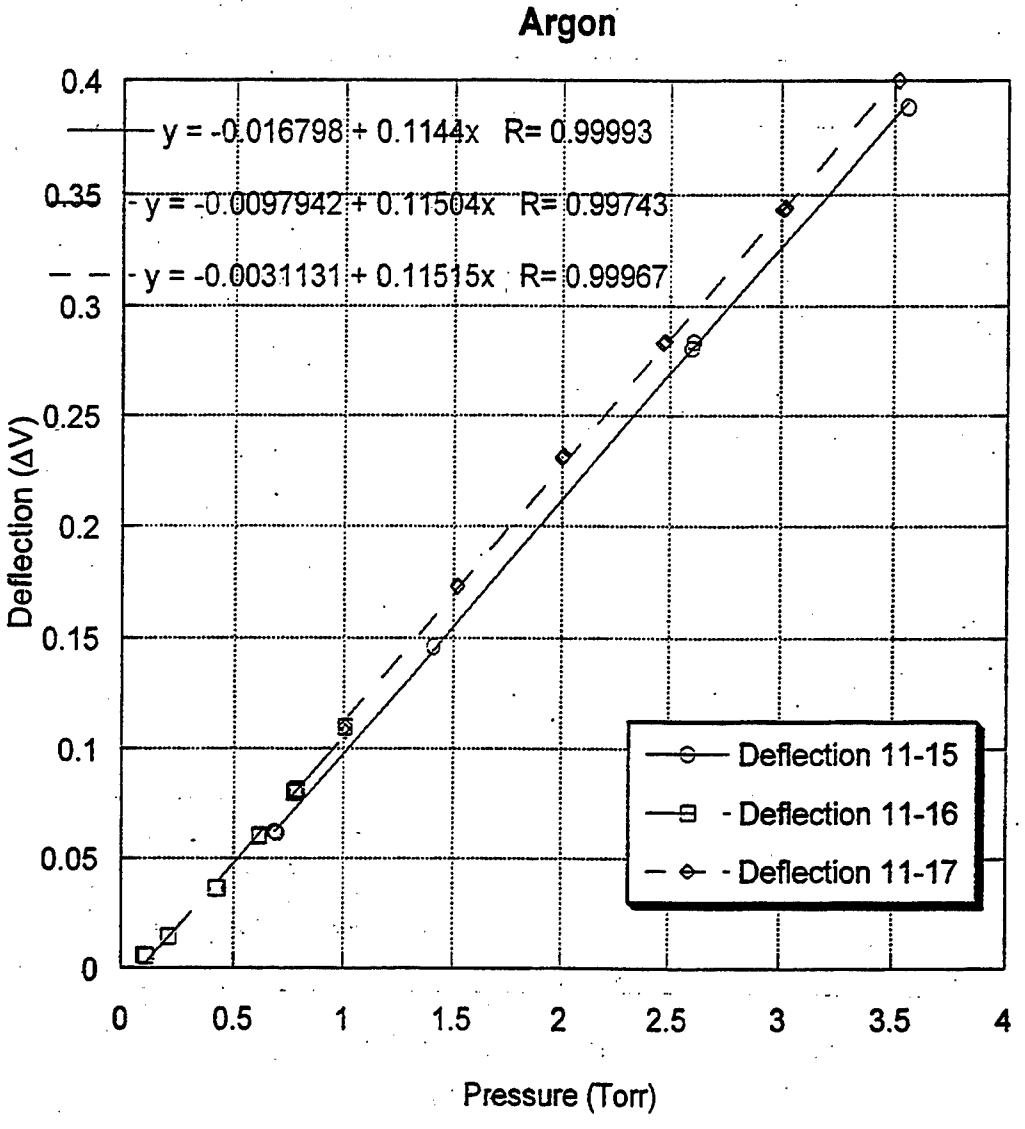
Argon
y = -0.016798 + 0.1144x R= 0.99993
y = -0.0097942 + 0.11504x R= 0.99743
y = -0.0031131 + 0.11515x R= 0.99967
Deflection (ΔV)
0.4
0.35
0.3
0.25
0.2
0.15
0.1
0.05
0
0
0.5
1
1.5
2
2.5
3
3.5
4
Pressure (Torr)
Deflection 11-15
Deflection 11-16
Deflection 11-17

Fig.6

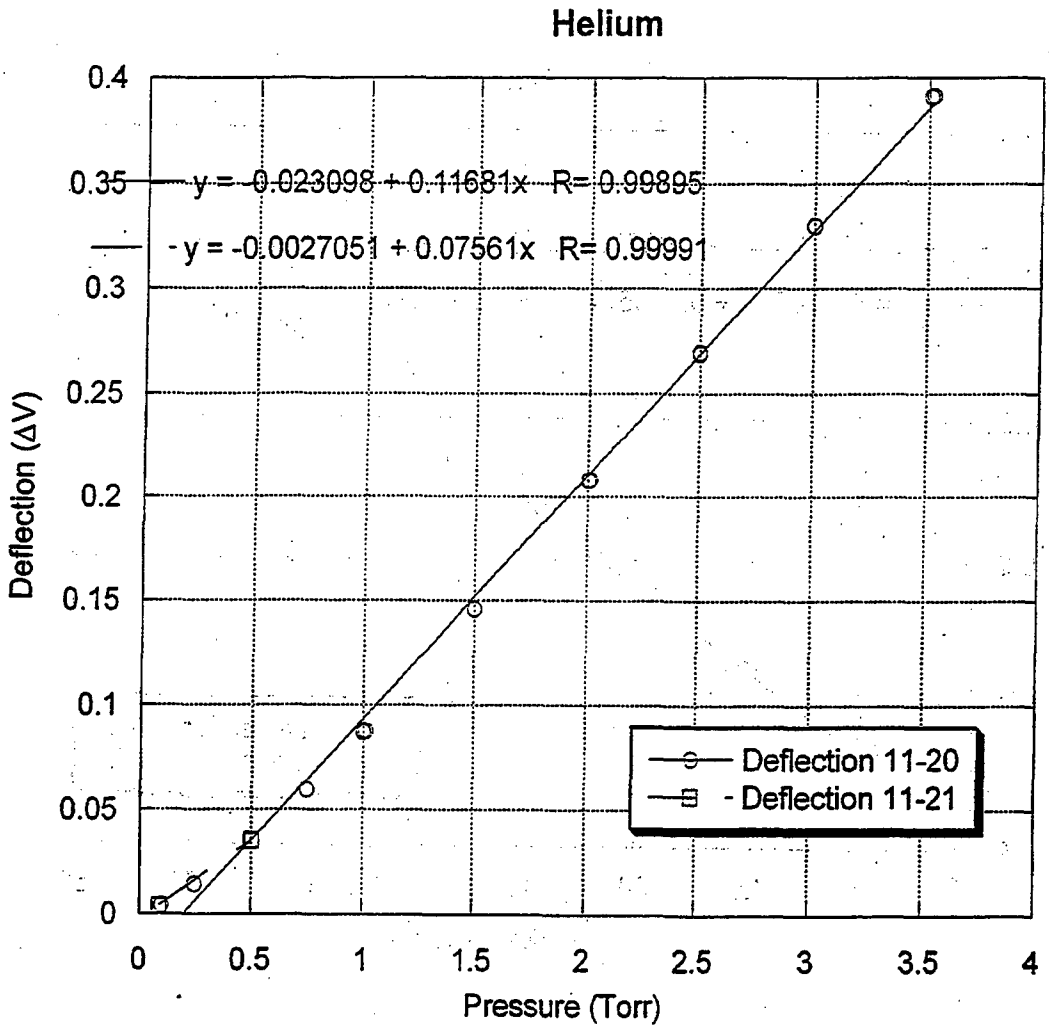
Helium
y = -0.023098 + 0.11681x R= 0.99895
y = -0.0027051 + 0.07561x R= 0.99991
Deflection (ΔV)
Pressure (Torr)
Deflection 11-20
Deflection 11-21
0.4
0.35
0.3
0.25
0.2
0.15
0.1
0.05
0
0
0.5
1
1.5
2
2.5
3
3.5
4

Fig. 7

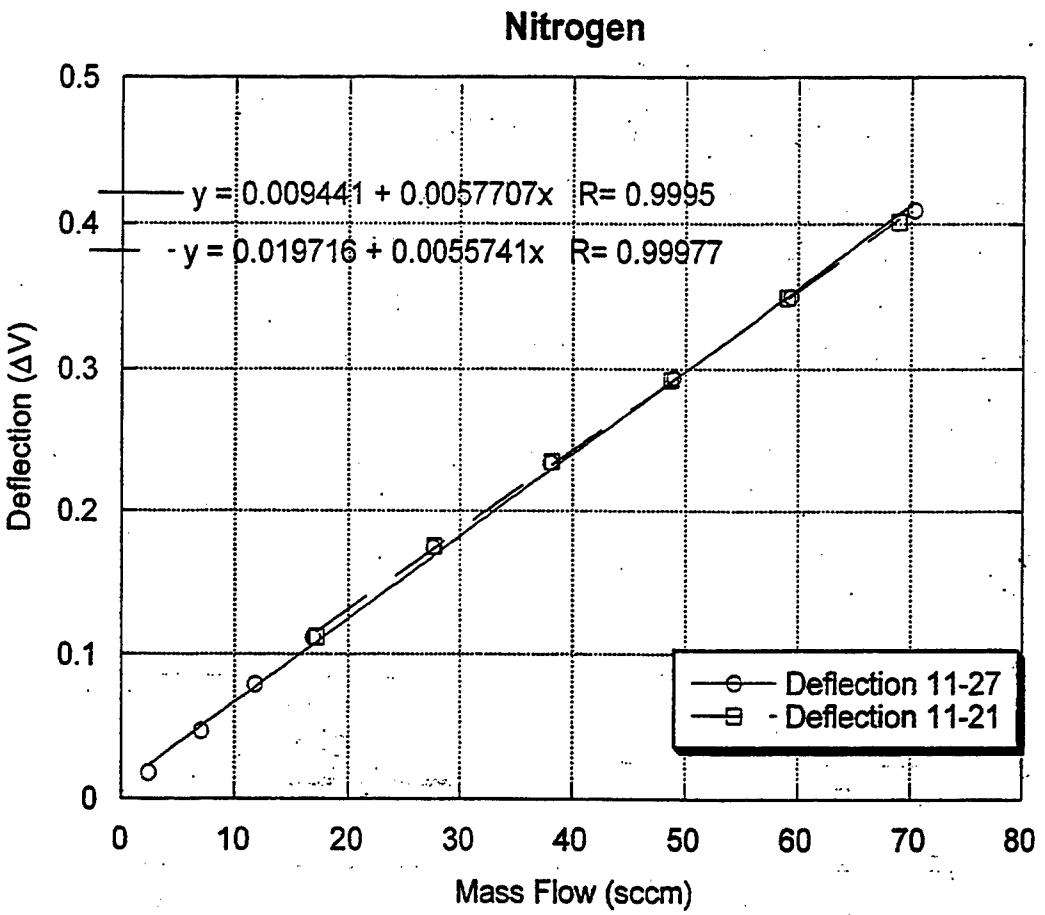
Nitrogen
y = 0.009441 + 0.0057707x R= 0.9995
- y = 0.019716 + 0.0055741x R= 0.99977
Deflection (ΔV)
0.5
0.4
0.3
0.2
0.1
0
0
10
20
30
40
50
60
70
80
Mass Flow (sccm)
Deflection 11-27
- Deflection 11-21

Fig. 8

Suggestion: If possible, move text box/legend away from caption.

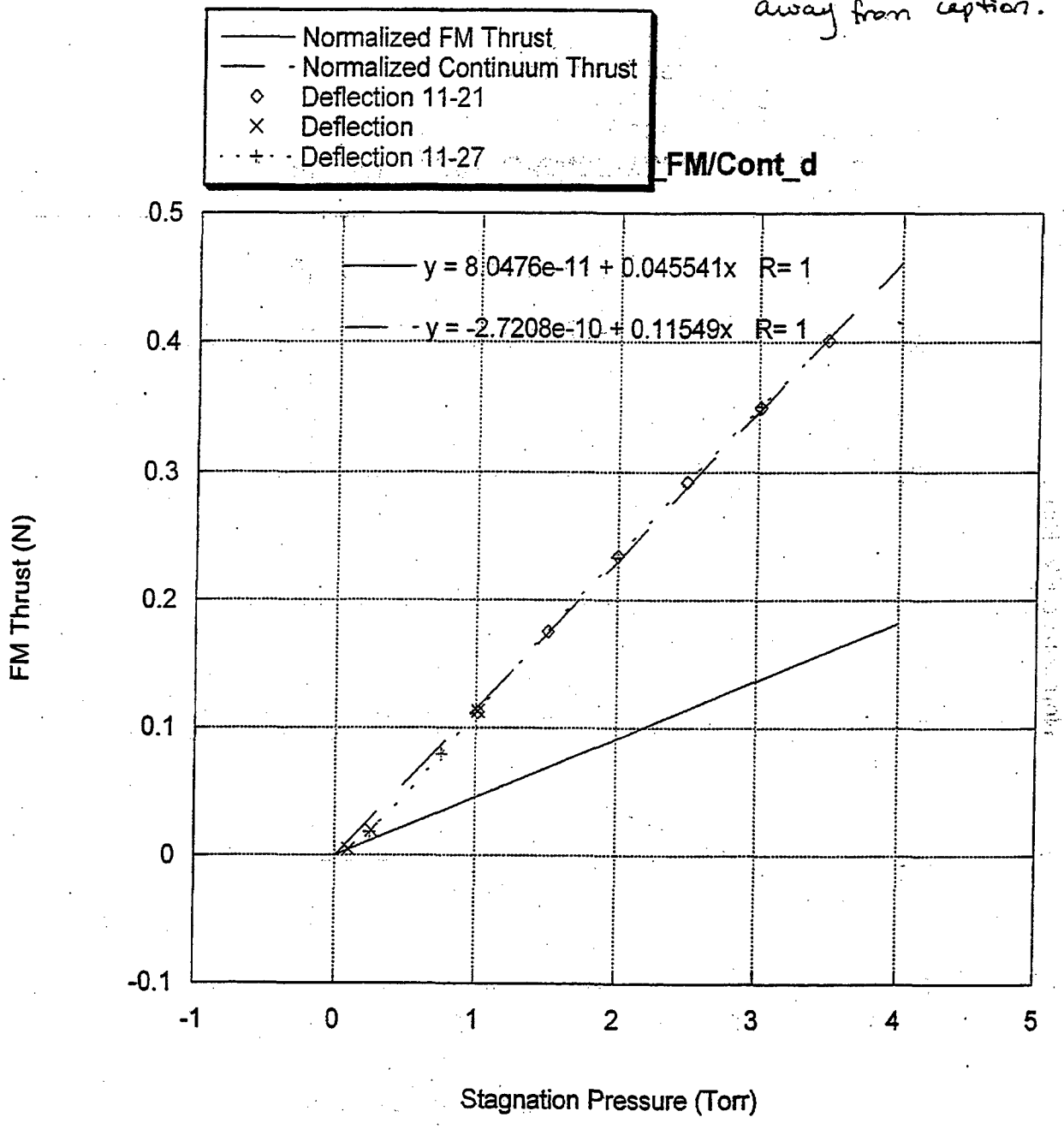

Fig. 9(a)

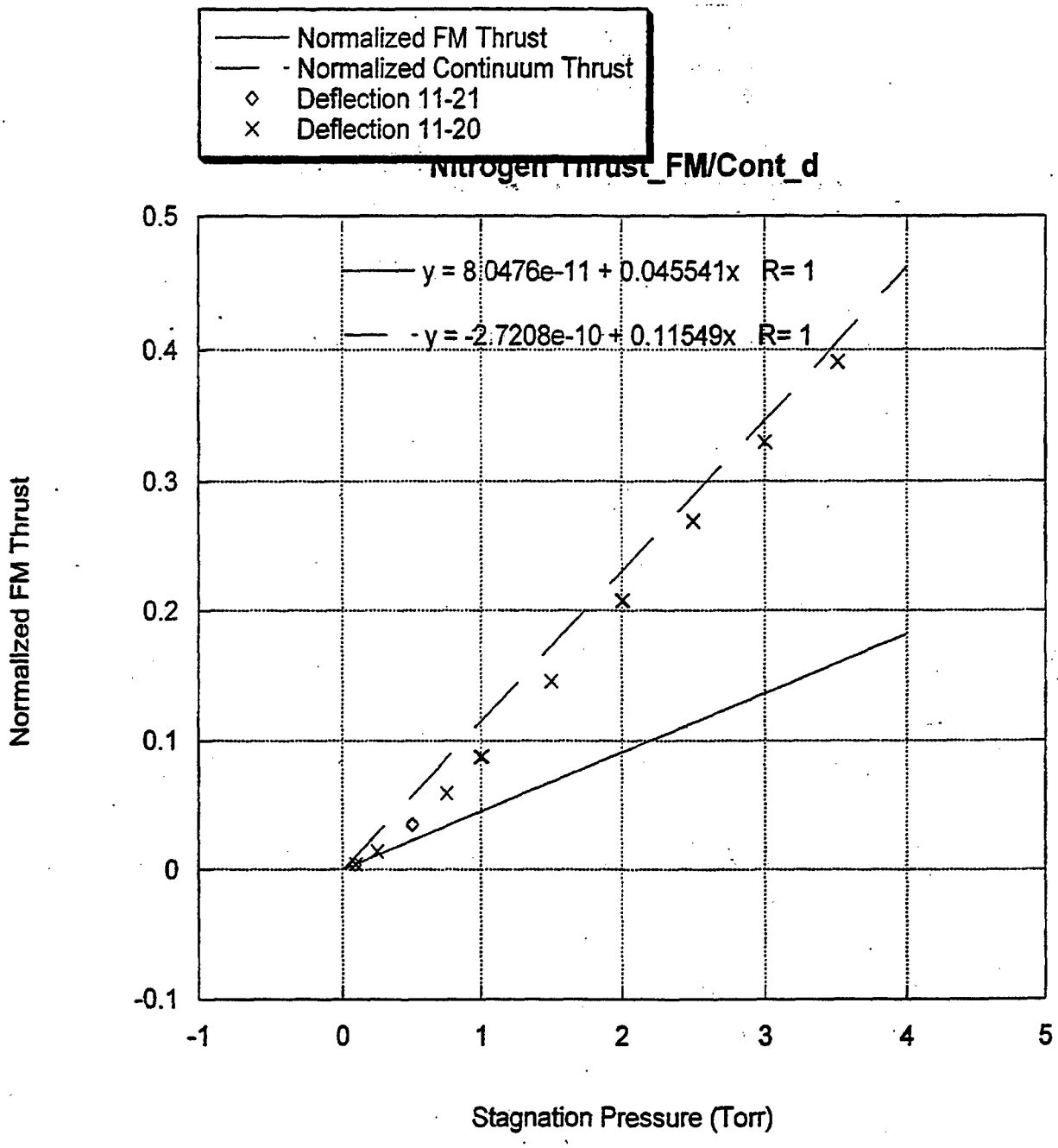
Normalized FM Thrust
Normalized Continuum Thrust
Deflection 11-21
Deflection 11-20
Nitrogen Thrust_FM/Cont_d
y = 8.0476e-11 + 0.045541x R= 1
y = -2.7208e-10 + 0.11549x R= 1
Normalized FM Thrust
Stagnation Pressure (Torr)
0.5
0.4
0.3
0.2
0.1
0
-0.1
-1
0
1
2
3
4
5

Fig. 9(b)

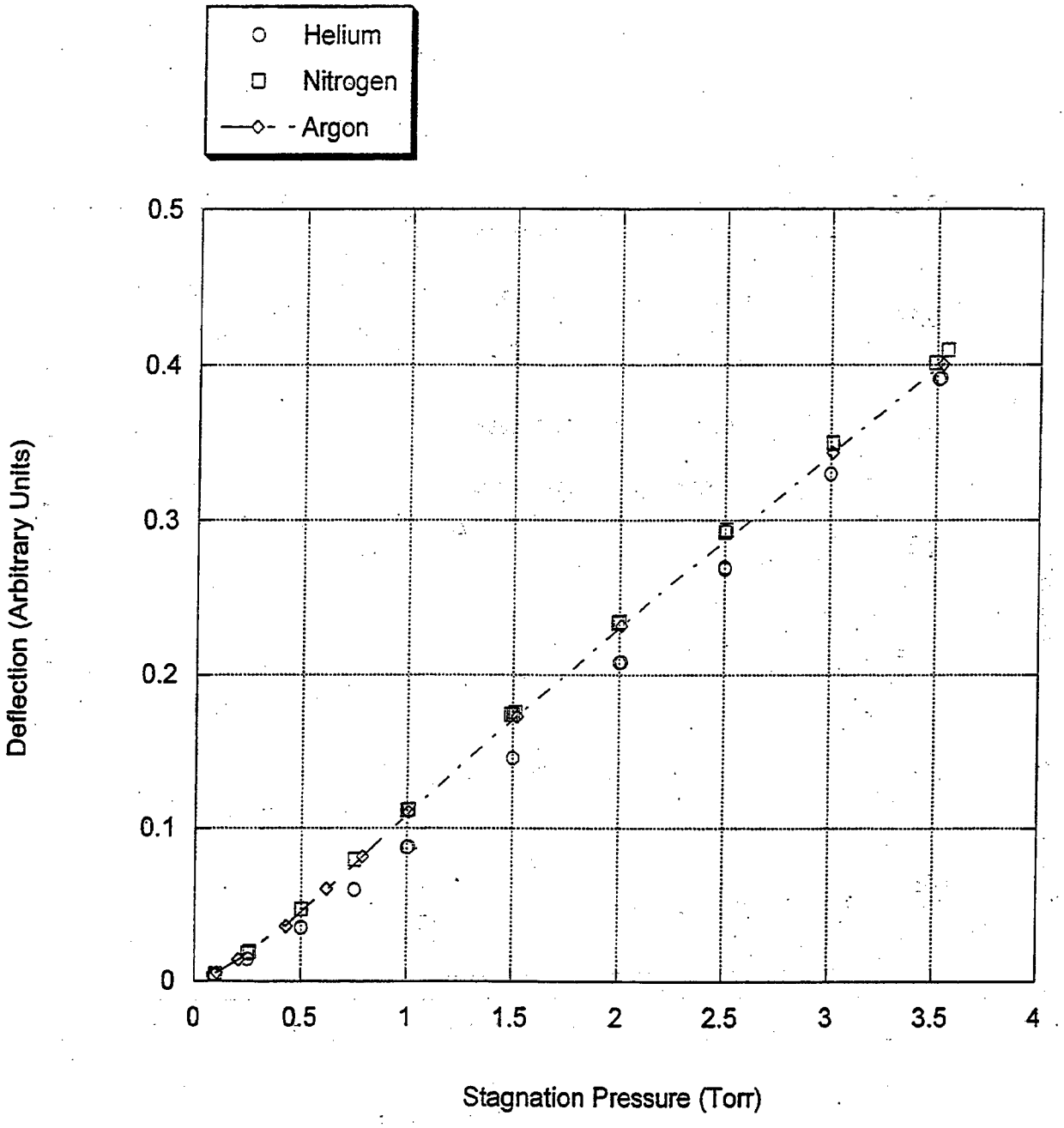
Helium
Nitrogen
Argon
Deflection (Arbitrary Units)
0.5
0.4
0.3
0.2
0.1
0
0
0.5
1
1.5
2
2.5
3
3.5
4
Stagnation Pressure (Torr)

Fig. 10

Legend ?

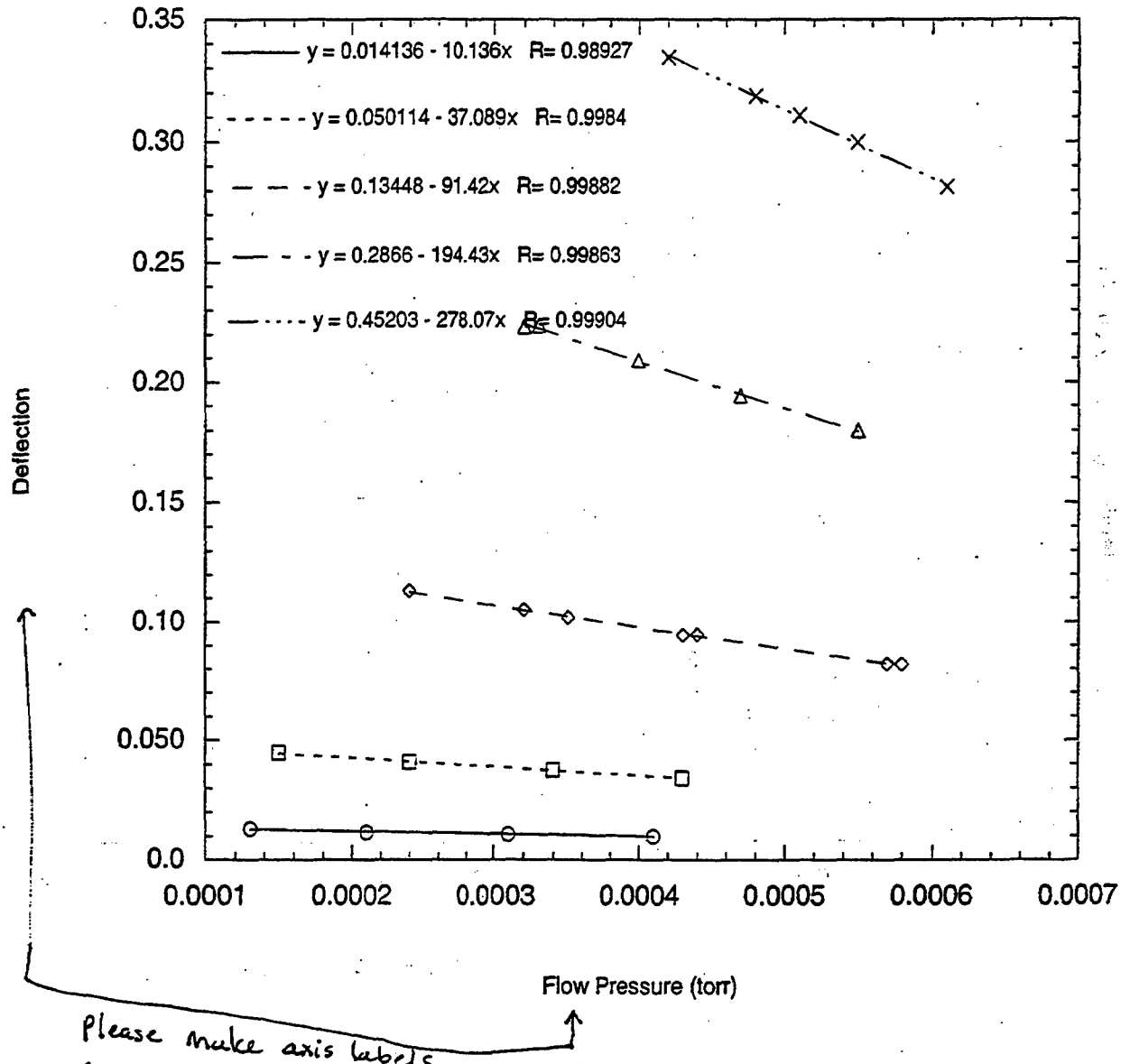

Please make axis labels same size text as labels in other figures

Fig. 11

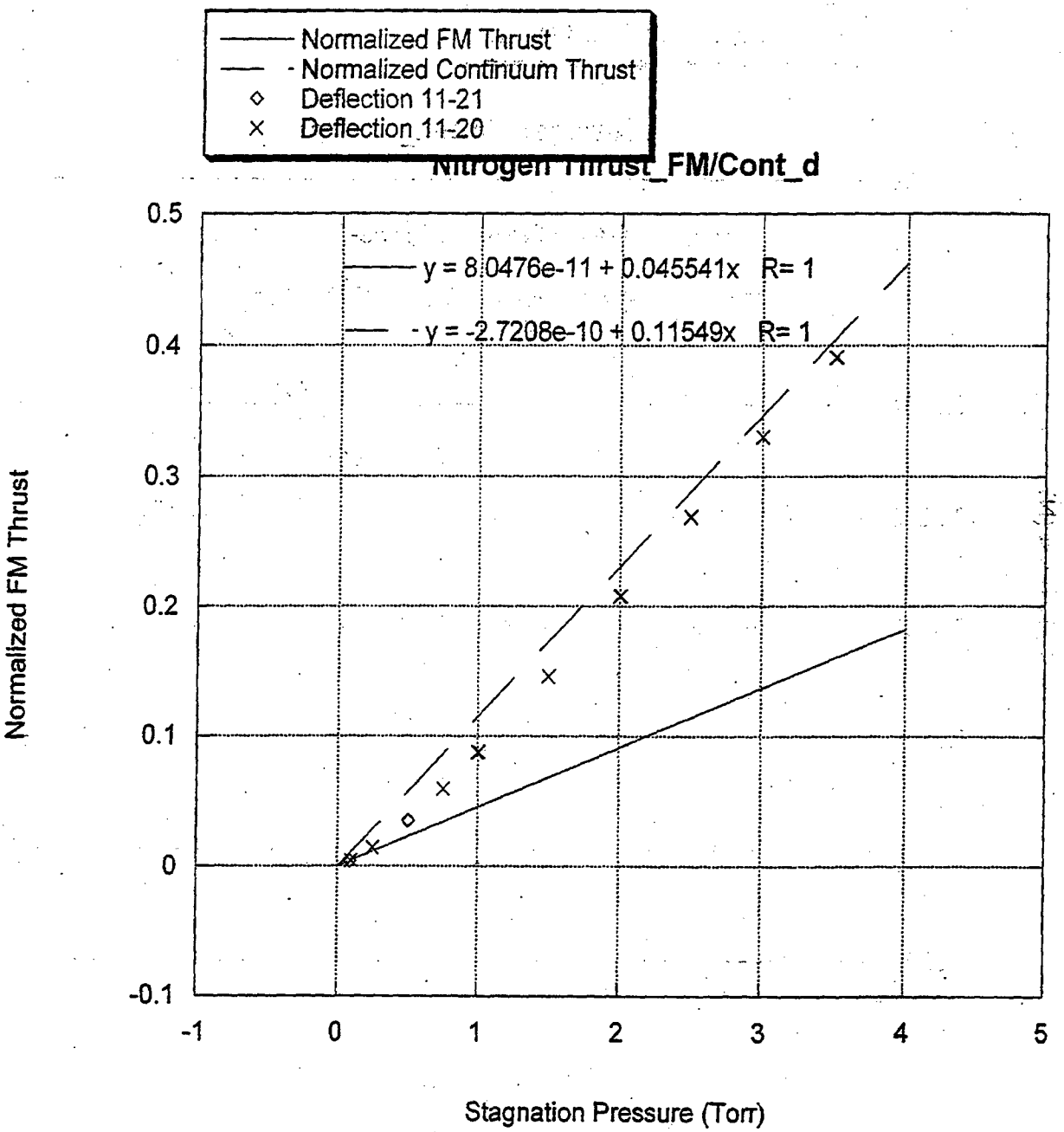
Normalized FM Thrust
Normalized Continuum Thrust
Deflection 11-21
Deflection 11-20
Nitrogen Thrust_FM/Cont_d
y = 8.0476e-11 + 0.045541x R= 1
y = -2.7208e-10 + 0.11549x R= 1
Normalized FM Thrust
Stagnation Pressure (Torr)
0.5
0.4
0.3
0.2
0.1
0
-0.1
-1
0
1
2
3
4
5

Fig. 12

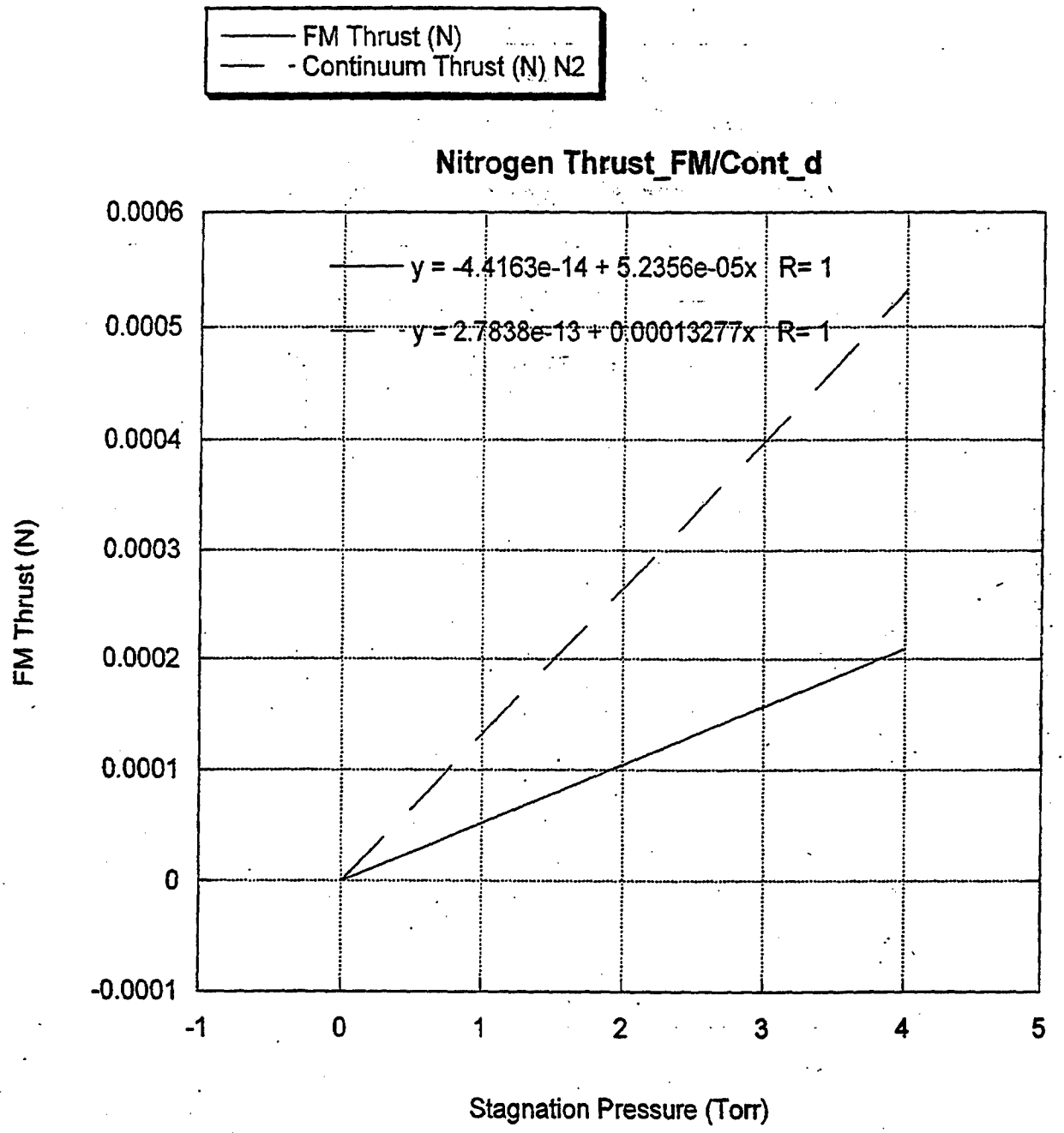
FM Thrust (N)
- Continuum Thrust (N) N2
Nitrogen Thrust_FM/Cont_d
y = -4.4163e-14 + 5.2356e-05x R= 1
y = 2.7838e-13 + 0.00013277x R= 1
0.0006
0.0005
0.0004
0.0003
0.0002
0.0001
0
-0.0001
FM Thrust (N)
-1
0
1
2
3
4
5
Stagnation Pressure (Torr)

Fig. 13

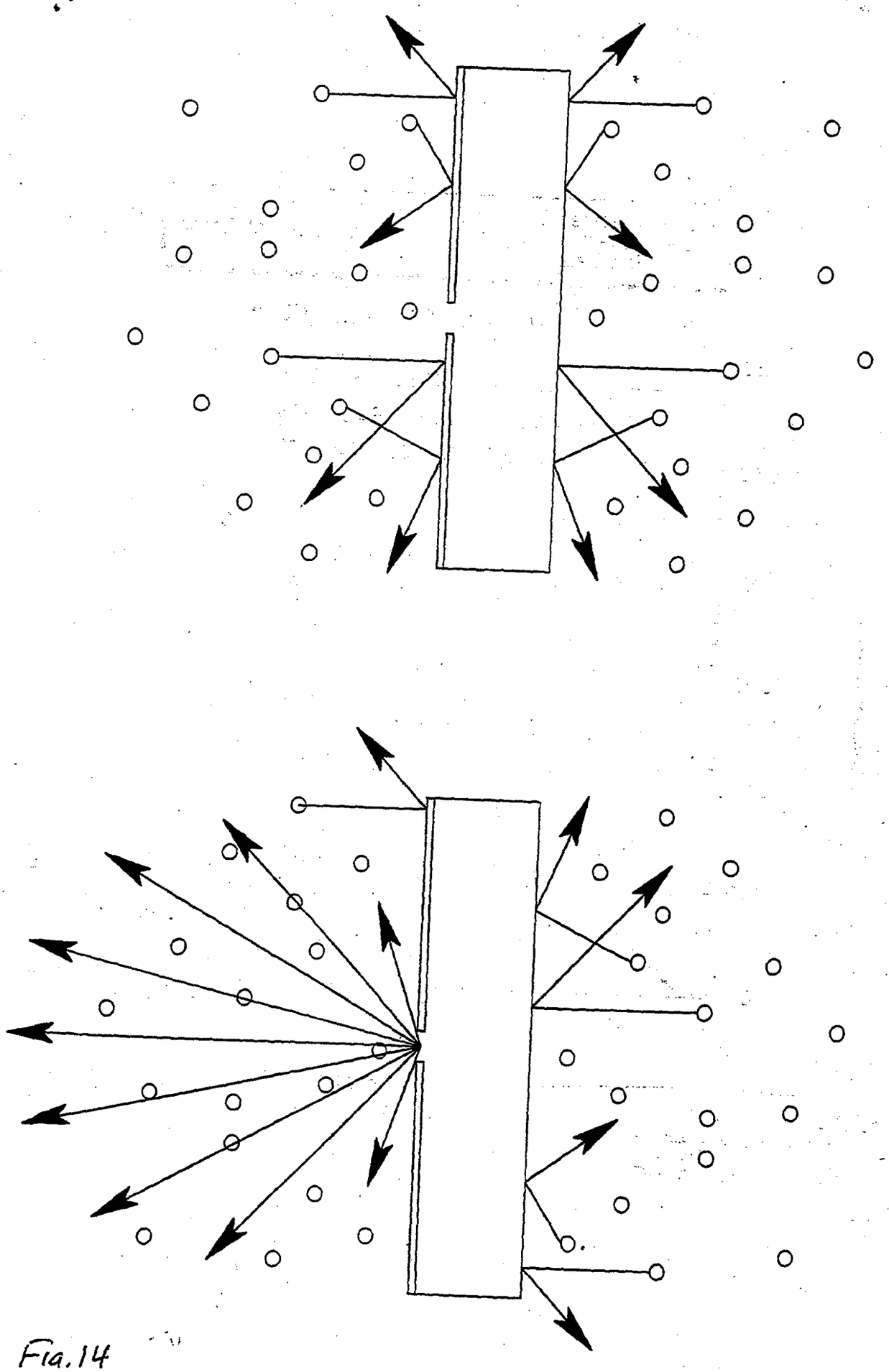

Fig. 14

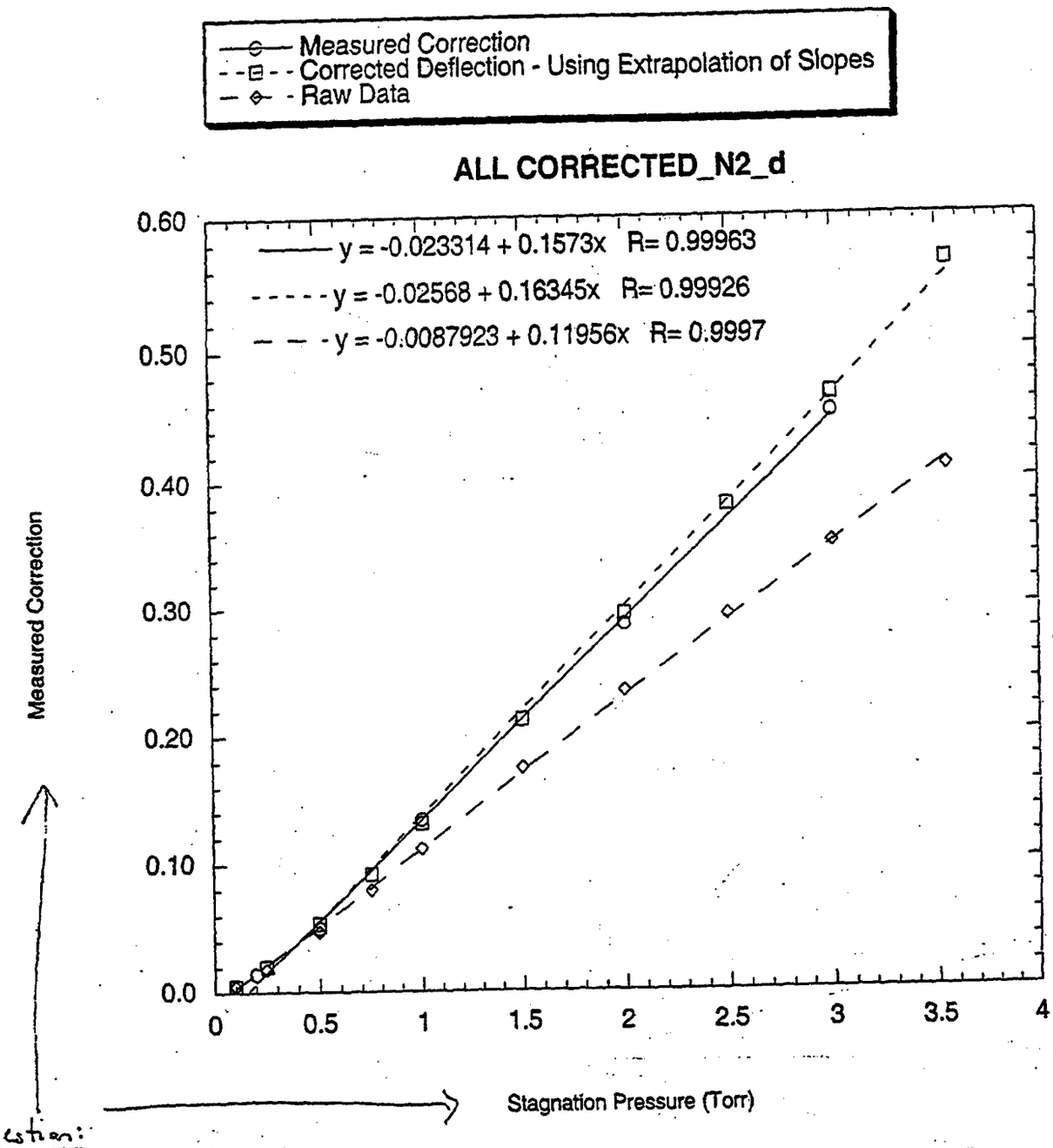

Suggestion:
Make text a little bigger to be consistent with other figures.

Fig. 15